Memory effect in composites of liquid crystal and silica aerosil

Sabrina Relaix
Department of Physics, McGill University, Montreal, Quebec, Canada H3A 2T8 and
Department of Chemistry, McGill University, Montreal, Quebec, Canada H3A 2K6

Robert L. Leheny
Department of Physics and Astronomy, Johns Hopkins University, Baltimore, Maryland 21218, USA

Linda Reven
Department of Chemistry, McGill University, Montreal, Quebec, Canada H3A 2K6

Mark Sutton
Department of Physics, McGill University, Montreal, Quebec, Canada H3A 2T8
(Received 7 September 2011; published 27 December 2011)

Aerosil silica nanoparticles dispersed in a liquid crystal (LC) possess the interesting property of keeping memory of an electric- or magnetic-field-induced orientation. Two types of memory have been identified: thermally erasable memory arising from the pinning of defect lines versus a "permanent" memory where the orientation persists even after thermal cycling the samples up to the isotropic phase. To address the source of the latter type of memory, solid-state nuclear magnetic resonance spectroscopy and conventional x-ray diffraction (XRD) were first combined to characterize the LC orientational order as a function of multiple in-field temperature cycles. Microbeam XRD was then performed on aligned gels of different concentrations to gain knowledge of the structural properties at the origin of the memory effect. No detectable anisotropy of the gel or significant breaking of silica strands with heating ruled out the formation of an anisotropic silica network as the source of the permanent memory as previously proposed. Instead, support for a role of the surface memory effect, well known for planar substrates, in stabilizing the permanent memory was deduced from "training" of the composites, that is, optimizing the orientational order through the thermal in-field cycling. The ability to train the composites is inversely proportional to the strength of the random-field disorder. The portion of thermally erasable memory also decreases as the silica density increases. We propose that the permanent memory originates from the surface memory effect operating at points of intersection in the silica network. These areas, where the LC is strongly confined with conflicted surface interactions, are trained to achieve an optimized orientation and subsequently act as sites from which the LC orientational order regrows after zero-field thermal cycling up to the isotropic phase.

DOI: 10.1103/PhysRevE.84.061705 PACS number(s): 61.30.Pq, 61.30.Gd, 61.05.cf

I. INTRODUCTION

Liquid crystals (LCs) mixed with aerosil or incorporated into silica aerogels have been widely studied experimentally and theoretically as these silica structures impose a random disorder on the LC. Due to the LC soft elasticity, high sensitivity to surface interactions, as well as control over the silica density, LC-aerosil dispersions are good physical models for the effect of quenched random disorder on critical phase transitions, such as the nematic (N) to smectic-A one. The other notable characteristic of this system is a memory effect that is reported to be almost permanent [1,2].

A memory, or stability, of the LC orientation was first noticed for N-aerosil dispersions that were found to retain an electric-field-induced preferential orientation after removal of the field in the N phase [3,4]. Subsequent studies reported the influence of the concentration and hydrophobicity of the silica nanoparticles on the extent of the memory as quantified by light transmission [5]. The effect was found to be maximized for low silica concentration above the gelation threshold where the ratio of transmitted light after and during the application of the field was the largest. The creation of an anisotropic network and its stabilization by the LC elastic forces was put forth to explain the effect [5]. The memory of the LC orientation was also observed in nematic LCs confined to 3-μm Millipore membranes and filled by hydrophobic aerosil by Bellini and co-workers, which they thoroughly studied primarily by means of turbidity measurements and by comparison with randomly pinned spins models [6,7]. They reported the loss of orientational stability by heating the samples to the isotropic phase in zero field.

Another type of orientational memory is observed in LC films in contact with a surface, where a single molecular layer at the interface can dictate the director orientation throughout the LC bulk [8]. This memory is often referred to as the surface memory effect and describes the preservation of the LC initial ordered texture after heating the samples up to the isotropic phase, sometimes even up to 50 °C above the phase transition [9].

A permanent memory was also observed for smectic-A–hydrophilic-aerosil samples [10], allowing analysis by neutron or x-ray scattering (XRD) through diffraction by the smectic density wave [11]. The orientation was selected by cooling the mixtures from the isotropic phase in a magnetic field, which is preferred over the electric field to avoid any ion accumulation and screening effects. The restoration of the

smectic alignment after prolonged annealing in the isotropic phase with sonication and no applied field was reported [10].

The origin of both the permanent and thermally erasable memories has been the subject of a range of theoretical and experimental studies, but no clear consensus has been reached. Anisotropy of the silica network was first proposed [2,5] due to the weak, thixotropic nature of the network at low aerosil concentrations. However, simulations and experimental work by Bellini and co-workers indicate that anisotropy is not required for inducing at least thermally reversible memory effects. Instead, the pinning of defect lines was found to be sufficient for inducing the memory of a preferential orientation [6]. In addition, no anisotropy in the small-angle x-ray scattering (SAXS) of Sm-aerosil samples cycled at least 100 times in a magnetic field was found [12], which raises doubt about the possibility of anisotropy in the network. Recent computer simulations by Bellini and co-workers indicate that the memory has its origin in the topology of the confining surface and is predicted to be maximized by a periodic bicontinuous cubic structure [13]. Geometrically induced frustration leads to numerous metastable topological defect lines in the confined LC that are greatly stabilized by looping around the interconnected spaces [13]. Since any pinned defect lines induced by the confinement topology of the silica network should be destroyed by heating to the isotropic phase, the mechanism of the permanent memory of the LC-aerosil dispersions remains unresolved.

In this paper we revisit the role of anisotropy versus pinned defects by combining solid-state nuclear magnetic resonance (NMR) with x-ray diffraction (XRD). First, "training" of the LC-aerosil dispersions by in-field cooling is monitored as a function of the number of temperature cycles and silica concentration. Hydrophilic aerosil was used to optimize the memory effect [10]. The structure and spatial heterogeneity in the LC ordering on the micrometer scale was then probed using microbeam x-ray diffraction. Zero-field *in situ* temperature cycles were carried out to test the stability of the memory effect as a function of the aerosil concentration. Finally, SAXS was also performed on aligned samples to search for anisotropy of the silica structure.

II. EXPERIMENT

A. Sample preparation and characteristics

The well-studied LC 4-*n*-octyl-4′-cyanobiphenyl (8CB) exhibits two LC phases and presents the following transition temperatures: the isotropic (I) to nematic transition is at ∼312.6 K, the N to smectic transition is at ∼305.6 K, and the smectic to crystal transition is observed at ∼271 K on cooling [14]. The 8CB was purchased from Frinton Laboratories, Inc. and used without further treatment. In prevision of the NMR study, a portion of pure 8CB (∼35 wt.%) was replaced by 8CB deuterated on the first carbon position along the hydrocarbon chain (α position). This changes neither the transition temperatures nor the interaction with the aerosil.

The aerosil was purchased from Degussa Corp. and consists of 70-Å-diam SiO_2 spheres. The type A300, used in this study, is strongly hydrophilic (5 OH groups per nm^2) and hydrogen bonds are formed in between the silica spheres and with the cyano group of 8CB molecules, as has been observed by Fourier-transform infrared spectroscopy studies [15]. Mixtures of 8CB and aerosil were prepared in the vein of a well-established technique using solvent evaporation [16]. The aerosil was first dried under vacuum at ∼150 °C for 24 h before being mixed with high-purity acetone to obtain ∼0.01 g cm^{-3} of suspension. The stock solution was then sonicated for 20 min with an ultrasonic probe to ensure complete dissolution of the aerosil. The desired amount of 8CB and deuterated 8CB was weighted so that the weight in deuterated 8CB was ∼0.1 g and the total weight in LC was ∼0.3 g. The desired amount of stock solution was then added to the LC and additional high-grade acetone was added to the solution. The evaporation of the solvent was then performed in three steps. The first step consisted in letting the solvent evaporate slowly at room temperature with a constant and mild stirring under a flow of argon until the suspension was mostly dry (usually around 1 h). A first evaporation under vacuum was done at room temperature for 1 h at 10 mtorr. The sample was then kept around 55 °C, in the LC isotropic phase, for at least 12 h under a vacuum of ∼2 mtorr and constant stirring. The absence of acetone in the solution was checked by solid-state NMR: No isotropic component at room temperature was observed, nor any significant shift in the LC transition temperature as compared to the literature data on the 8CB-aerosil mixture.

The four densities probed in this study ranged from $\rho_s =$ 0.007 g of silica per cm^3 of LC (abbreviated by g cm^{-3}) to $\rho_s = 0.091$ g cm^{-3}. This corresponds to a volume fraction in silica of 0.33% to 4.17%. Studies on LC-aerosil systems have consistently found two critical densities that define three regions of different characteristics [2,16]. For ρ_s smaller than ∼0.01 g cm^{-3} the aerosil strands are not linked together in a percolating three-dimensional (3D) structure and the aerosil aggregates act as impurities in the LC environment. This is defined as the no-gel regime. For ρ_s between ∼0.01 and ∼0.1 g cm^{-3} the silica particles form a soft 3D thixotropic gel that can anneal on relatively short time scales. It is proposed that the hydrogen bonds can easily break in this regime, leading to a rearrangement of the silica strands [2]. This regime is known as the soft-gel regime. Finally, for densities above ∼0.1 g cm^{-3}, the aerosil forms a densely packed gel, which defines the stiff-gel regime that is more comparable to aerogels. Our lowest-density sample belongs to the no-gel regime, while the other three ($\rho_s = 0.035$, 0.059, and 0.091 g cm^{-3}) span the soft-gel regime. The characteristics of the samples probed are summarized in Table I.

The mixtures were introduced into rectangular homemade Teflon cells, with Kapton windows for compatibility with x-ray scattering analyses. The external dimensions of the cells were ∼1.5 cm (height) × 1 cm (width) × 7 mm (thickness). The corresponding amount of material was ∼1.1 cm (height) × 6 mm (width) and a thickness close to 1.8 mm, as desired for optimized x-ray scattering in transmission mode at 7.35 keV.

For the SAXS data, the sample of 8CB with 0.059 g cm^{-3} of aerosil was analyzed as well as two other samples: one in the soft-gel regime ($\rho_s = 0.03$ g cm^{-3}) and one in the stiff-gel regime ($\rho_s = 0.2$ g cm^{-3}). The last two mixtures were introduced into a circular hole of 6 mm diameter in aluminum blocks of dimensions 1 in. × 1 in. × 1.3 mm, covered with Kapton.

TABLE I. Characteristics of 8CB-aerosil dispersions used in this study. The mean void size is defined as $l_0 = 2/a\rho_s$ [16], with $a = 300\ m^2\ g^{-1}$ the specific silica area, and $\xi_\parallel$ is the average smectic correlation length obtained from the fit of the XRD line shapes at 25 °C before the zero-field temperature cycle. It is approximately four times larger than the mean void size, showing that the pores are interconnected.

ρ_s (g cm^{-3})	Aerosil volume fraction (%)	l_0 (Å)	$\xi_\parallel$ (Å)
0.007[a]	0.33		12867
0.035	1.63	1924	7855
0.059	2.76	1124	5339
0.091	4.17	734	3209

[a]No-gel regime.

B. Nuclear magnetic resonance

The samples were cycled in temperature in the chamber of a solid-state NMR Varian/Agilent VNMRS-400. The spectra were obtained by a $(\pi/2)_x$-$(\pi/2)_y$ echo pulse sequence at the Larmor frequency for deuterium of 61.4 MHz, in a 9.4-T magnet. The recycling delay was 0.1 s and 5000 scans were acquired for each spectrum.

C. X-ray diffraction

The x-ray diffraction data were collected using a 2-kW sealed x-ray copper tube with a point scintillator detector and a triple crystal spectrometer in the non-dispersive geometry [17]. The monochromator and analyzer were germanium (111) crystals. The beam size was approximately $1 \times 4\ mm^2$. A four-circle goniometer enabled us to vary the orientation of the samples with respect to the scattering plane and thereby characterize the quality of the LC orientational order through mosaic scans (θ rocking curves) on the smectic Bragg peak.

D. Microbeam x-ray diffraction

The microbeam XRD experiments were conducted at sector 8-ID of the Advanced Photon Source at Argonne National Laboratory, at beamline 8-ID-G. A beam of 7.35-keV x-rays was selected and the measurements were performed in transmission geometry. The single-bounce monochromator used was a crystal of silicon (111). The beam size was $20 \times 20\ \mu m^2$. The scattering intensity, recorded by a direct illumination CCD area detector, was measured over a scattering vector range centered on the smectic scattering vector $q_0 \sim 0.1994\ Å^{-1}$. The pixels were $20 \times 20\ \mu m^2$ in size and each pixel corresponded to a variation in q of $3.24 \times 10^{-5}\ Å^{-1}$, permitting us to achieve high resolution. The flux of the incoming beam was $\sim 2.3 \times 10^9$ photons/s. The exposure time was varied depending on the silica concentration. Exposure times of 0.2 and 1 s were usually chosen, depending on the degree of alignment of the sample, to prevent overexposure on the CCD detector.

Cycles in temperature were performed *in situ* using a copper oven designed to fit our cell dimensions. The heating source was provided by a cartridge heater incorporated in the base of the copper block and the control loop was done using a platinum resistance thermometer (PRT) also fit in a hole in the copper block, close to the base of the sample. The temperature was measured using another PRT placed near the top of the sample to measure more accurately the temperature experienced by the sample and the temperature gradient across it. The maximum temperature gradient measured at 46 °C was 0.049 over a distance of 12 mm and it was only 0.008 at 25 °C. The copper block was positioned on a copper base that was water cooled to ensure good cooling rates. The temperature controller was from LakeShore Cryogenics. The cycles were made at 1 K/min and the variation in intensity and correlation length observed on the CCD detector could be monitored as a function of temperature and the number of cycles. The cycles were done in the absence of a magnetic field except for the no-gel sample (0.007 g cm^{-3}) where a 0.5-T magnetic field was used. The magnetic field was obtained through two $(1 \times 1 \times 0.5)$-in.^{3} neodymium iron boron magnets held together by an iron yoke designed to fit on the copper oven.

E. Small-angle x-ray scattering

Small-angle x-ray scattering experiments were performed at beamline 8-ID-I of the Advanced Photon Source. The measurements were performed in transmission geometry using a 7.35-keV beam. A two-bounce germanium (111) monochromator was used. The beam size was $20 \times 20\ \mu m^2$ and the incoming flux was $\sim 3.7 \times 10^9$ photons/s. The q range probed spanned from 0.0016 to 0.051 Å^{-1}, which corresponds to length scales from 123 to 3935 Å. The incident light was partially coherent, with a contrast factor β (ratio of the coherence volume to the scattering volume) of $\sim 30\%$.

III. ALIGNMENT PROCEDURE

A. In-field temperature cycling: NMR and XRD data

Following preparation, the samples were aligned in a magnetic field through repetitive temperature cycles using the NMR spectrometer. The NMR studies had a dual purpose: to align the samples in a high magnetic field and to characterize their degree of alignment. The cycles were performed at 1 K/min between 38 °C and 43 °C (through the N-I transition) and the degree of alignment of the samples was checked periodically at 25 °C by NMR and XRD.

Nuclear magnetic resonance analysis of LC samples is a powerful method to obtain the orientational distribution of domains of molecules with respect to the magnetic field. The degree of alignment of the samples was determined from a fit to the NMR spectra. In the case of a well-aligned nematic sample, the spectrum consists of two sharp absorption lines with a frequency spacing:

$$\Delta\nu = \nu_+ - \nu_- = \Delta\nu_\circ S\left(\frac{3\cos^2\theta - 1}{2}\right). \quad (1)$$

Here $\Delta\nu_\circ$ is the quadruple splitting related to the deuterium quadrupole moment, S is the nematic scalar order parameter, and θ is the angle between the molecules director and the magnetic field [18].

For a distribution of orientations, the spectrum is a weighted sum with the appropriate probability distribution.

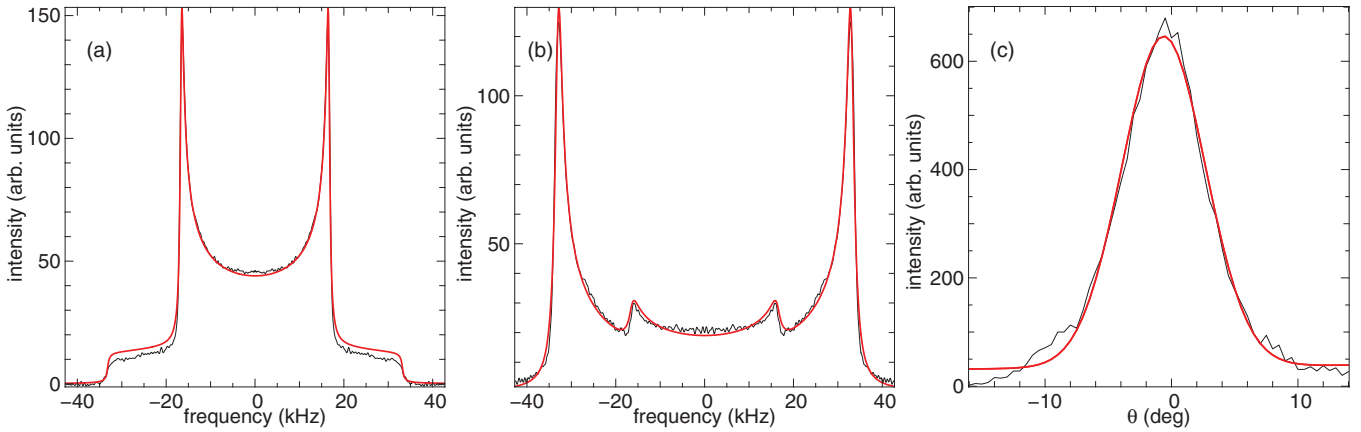

FIG. 1. (Color online) Symmetrized NMR spectra [thin (black) line] and their fits [thick (red) line]: (a) Pake pattern obtained for the sample of 8CB with 0.035 g cm^{-3} of aerosil before any in-field temperature cycle, $\Delta\nu/2$ = 33.2892 kHz, an intensity factor of 96.8, and a linewidth $\sigma_f = 0.010\nu$; (b) sample of 8CB with 0.059 g cm^{-3} of aerosil after 22 training cycles, $\Delta\nu/2$ = 33.1597 kHz, an intensity factor of 95.2, a Gaussian fraction $\alpha = 1$, and linewidths $\sigma_f = 0.021\Delta\nu$ and $\sigma_\theta = 28.3^\circ$. (c) An x-ray mosaic scan [thin (black) line] and its fit [thick (red) line] for a sample of 8CB with 0.035 g cm^{-3} of aerosil after 12 cycles and a full width at half maximum equal to 7.77°.

Furthermore, these NMR lines are broadened due to magnetic interactions between adjacent nuclei that can be approximated with a Lorentzian line shape [18]. The spectrum becomes the convolution of the probability density and the Lorentzian line shape $I(f - f')$ with linewidth σ_f [18]:

$$F(f) = \int_{-\infty}^{+\infty} I(f - f')p(f')df', \tag{2}$$

where p is the sum of the probabilities $p_\pm$,

$$p_\pm(f) = p(\theta)\frac{d\theta}{df_\pm}, \tag{3}$$

and $f_\pm$ are the reduced resonant frequencies defined as $f_\pm = \pm(3\cos^2\theta - 1)/2$ ($\theta = 0$ and $\pi/2$ correspond to $f = \pm 1$ and $\mp 1/2$, respectively).

In the case of a powder, where all orientations are equally present, the characteristic shape is known as the Pake pattern. It has shoulders at $\theta = 0$, that is, at $\Delta\nu \sim 66$ kHz, and sharp features $\theta = \pi/2$ or at $\Delta\nu/2 \sim 33$ kHz here [see Fig. 1(a)]. For a Pake pattern, the probability density that a molecule is at an angle θ from the magnetic field is $p_P(\theta) = \sin\theta/2$ [18]. Using the double-value nature with respect to θ, it follows that the Pake probability density is

$$p_P(f) \propto \frac{1}{\sqrt{2f + 1}} + \frac{1}{\sqrt{-2f + 1}}. \tag{4}$$

Figure 1(a) shows a typical Pake pattern and the fit obtained with three free parameters: a parameter taking into account the peak position in reduced frequency, an intensity factor as a multiplicative constant, and the linewidth of the broadening in frequency σ_f.

Given the probability distribution of the LC director orientation, a line shape can be determined, but inverting the process can be difficult. It is especially arduous to achieve for distributions sharply peaked near $\theta = 0^\circ$ as the line shape is insensitive to small variations around this angle that are hidden by the Lorentzian broadening in frequency of Eq. (2). We define the aligned nematic probability distribution [19] with a Gaussian $p_G(\theta) = C\exp[(-1 + \cos^2\theta)/2\sigma_\theta^2]$ having a normalization constant C and a line broadening of σ_θ, somewhat similarly to other director distributions found in the literature [20,21]. For the highest-density data (8CB with 0.091 g cm^{-3} of aerosil) and at large angular spreads, it was necessary to add a small component with a Pake distribution to better fit the NMR line shape. Defining α as the Gaussian fraction, the line shape is defined as

$$F(f) = \int_{-\infty}^{+\infty} I(f - f')[\alpha p_G(f') + (1 - \alpha)p_P(f')]df'. \tag{5}$$

To distinguish between the two broadening contributions σ_f and σ_θ, one should note that the director distribution is defined only for a reduced frequency between -1 and 1, that is, at frequencies in between the peaks of the full-splitting doublet. Reduced frequencies outside this range are modeled by the Lorentzian broadening in frequency σ_f and thus set the value of this parameter. It is usually of the order of 0.01–0.025$\Delta\nu$. A NMR spectrum and its fit for 8CB with 0.059 g cm^{-3} of aerosil are presented in Fig. 1(b).

In addition to providing information on the spacing of the smectic layering, x-ray scattering of LCs is an effective tool to determine the spatial orientation distribution of a set of planes through scans known as mosaic scans [22]. Mosaic scans are obtained by rotating the sample about an axis normal to the scattering plane passing by the layering direction or, in other words, by varying the angle θ between the incoming beam and the sample. This provides us with a measure of the degree of alignment of the smectic layers in a direction perpendicular to the layering. The scans were performed after the samples had been cycled several times in temperature in the NMR chamber. The mosaic scans were well fit with a Gaussian line shape [see Fig. 1(c)] and the full width at half maximum (FWHM) of the curves was compared with the angular spread obtained from the fit of the NMR spectra.

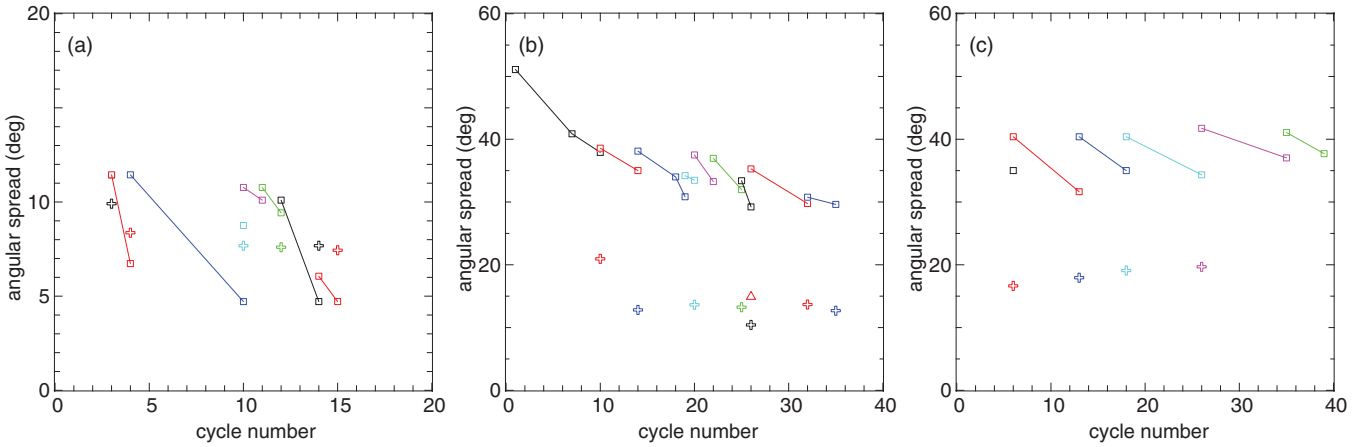

FIG. 2. (Color online) Angular spreads obtained through NMR (HWHM, squares) and XRD (FWHM, crosses) fits: (a) 8CB with 0.035 g cm^{-3} of aerosil, (b) 8CB with 0.059 g cm^{-3} of aerosil (the angular spread as determined by XRD after the zero-field temperature cycle is indicated by a triangle at cycle No. 26), and (c) 8CB with 0.091 g cm^{-3} of aerosil. Points connected by solid lines indicate that sample did not leave the NMR chamber.

B. Effect of silica concentration on LC alignment

The NMR and x-ray scattering experiments show how the memory effect develops. Figure 2 presents the half-width at half maximum (HWHM) of the angular distribution of the director obtained from the fit of the NMR line shapes ($2.35\sigma_\theta/2$) at 25 °C as a function of the number of cycles for the soft-gel samples. The lines connecting the square symbols indicate the cycles when the samples were left undisturbed in the NMR spectrometer and hence were kept in the 9.4-T field. The angular spread always decreased as the samples were cycled in the magnetic field. The breaks in the lines indicate the points when the samples were removed from the NMR spectrometer, sometimes to be brought to the x-ray diffractometer. The amount of time spent out of the field ranged from a few days to a few weeks. The sample temperature varied slightly during these times due to changes in room temperature, but was always maintained below the transition temperature to the N phase (except when intentionally heated through the transition; see the description at the end of the section).

The data for the no-gel sample is not shown as the orientational order is attained quickly in this case; one cycle in temperature is sufficient to obtain a full-splitting doublet with an angular spread too narrow to distinguish from the Lorentzian frequency broadening by NMR (therefore estimated to be below ±4°). Above the gelation threshold, the alignment improves with repeated cycles, as seen on the graphs of Fig. 2. The silica concentration deeply influences the effect of the magnetic field on the smectic alignment. Indeed, at the lowest silica concentration ($\rho_s = 0.035$ g cm^{-3}), 2 or 3 cycles are enough to achieve a strong alignment (angular spread below ±10°). As the concentration increases, the number of cycles needed to align the samples also increases. For $\rho_s =$ 0.059 g cm^{-3}, the angular spread reaches a plateau after ∼20 cycles, but is never as narrow as with the lower-concentration gel. For $\rho_s = 0.091$ g cm^{-3}, the angular spread is mostly constant after 6 cycles, but larger than for the other two samples. For pure 8CB, no cycle is needed; the magnetic field is powerful enough to overcome the viscoelastic forces that keep the smectic in a disordered, multidomain structure. These data are consistent with the picture that the degree of alignment of our samples increases with the number of cycles until it reaches an asymptotic plateau, where the number of cycles and the asymptotic degree of orientation depend on the silica concentration.

In agreement with the NMR data, the XRD data show that the degree of alignment of the samples depends on the silica concentration. The values obtained for the FWHM are somewhat different from what was obtained by fitting the NMR data, but the trend in the angular spread as a function of the number of cycles is similar. Even though the angular spreads obtained by NMR are probably erroneous due to the high sensitivity of the method to molecules oriented at 90° from the field, the fitting unambiguously demonstrates the training of LC orientational order in a qualitative manner. The difference in the values obtained from both methods may also come from a non-Gaussian distribution of director orientation as observed by fitting NMR spectra of polymer dispersed liquid crystal samples [23] and the fact that different quantities are probed: In the NMR case the nematic orientational distribution is probed, while the XRD analysis explores the orientational distribution linked to the smectic layering. As previously demonstrated [23], data acquisition with various rotation angles between the sample alignment direction and the magnetic-field direction should give better knowledge of the director distribution and the relative amounts of molecules free to rotate versus those frozen by the network.

Once a zero-field temperature cycle was done for the sample of 8CB with 0.059 g cm^{-3} of aerosil. At cycle No. 26, the sample was heated to 46 °C, where it stayed for 10 min before being cooled to room temperature with our homemade copper oven at 1 K/min (for details see Sec. II D). As can be seen in Fig. 2(b), the angular spread as determined by fitting the NMR spectra and the mosaic scans is mostly unaffected by this stay in the isotropic phase: It is larger than before the cycle, but the variation is not much stronger than when the sample is simply left out of the NMR spectrometer. After a certain number of cycles, the aligned samples were probed by synchrotron radiation.

IV. RESULTS

A. Stability of the memory: Microbeam XRD analysis

Once the samples were trained to have orientational memory, the structural properties of the samples were characterized using microbeam XRD before and after zero-field temperature cycles (except for the no-gel sample; see the description in Sec. II D). The local order was probed in a systematic way. The peak intensity and its distribution were recorded by an area detector for overlapping regions of the samples. The position of the samples between two data acquisitions was translated by 10-μm steps in the horizontal direction. The intensity distribution was fit by a 2D Lorentzian, with Lorentzian line shapes along the direction of increasing magnitude of q and along the azimuthal direction ϕ (arc of constant magnitude of q):

$$I(q,\phi) = \frac{4A\Gamma_\phi^2}{[1+4\xi_\parallel^2(q-q_0)^2]\left[1+4\Gamma_\phi^2(\phi-\phi_0)^2\right]}. \quad (6)$$

The amplitude A corresponds to an integrated intensity in ϕ [24]. The data are well fit by these line shapes, as can be seen in Fig. 3. The FWHM in the q vector direction is identified as the inverse of the smectic order parameter correlation length in the direction parallel to the nematic director $\xi_\parallel$ [11], which corresponds to the extent of the positional order in the direction of the density wave [22]. Along the arc of constant q, two mechanisms contribute to broadening the peak: One is related to the smectic correlation length in the direction perpendicular to the director $\xi_\perp$ and the other is linked to the mosaicity of the sample or, in other words, to the presence of misoriented smectic layers that scatter into different scattering planes [22]. The latter is the major contributor to the broadening in the azimuthal direction. The ratio of $\xi_\perp$ to $\xi_\parallel$ is also a well-documented quantity in bulk 8CB [25] as well as in trained 8CB-aerosil systems [12] (the ratio is close to 0.5 deep in the smectic phase in the latter case) and the obtained values of $\xi_\perp$ would not account significantly for the broadening observed along the arc. In a similar way to $\xi_\parallel$, we define Γ_ϕ as the inverse of the FWHM of the Lorentzian along the arc of constant q.

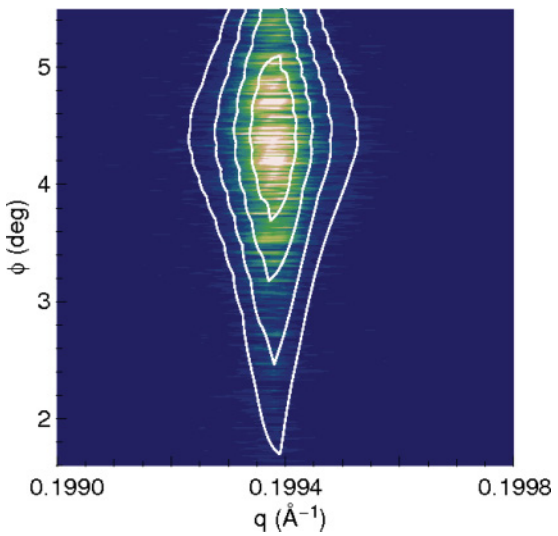

FIG. 3. (Color online) Image recorded on the CCD detector, showing the scattering from a (20 × 20)-μm^2 region of 8CB with 0.059 g cm^{-3} of aerosil at 25 °C, before the zero-field temperature cycle. The white lines are contour plots of the fit by a 2D Lorentzian with a FWHM in the parallel direction of $1/\xi_\parallel = 7.51 \times 10^{-5}$ Å^{-1} and in the perpendicular direction of $1/\Gamma_\phi = 1.48°$. The white lines indicate the FWHM, one-quarter, one-eighth, and one-sixteenth of the peak. The speckled appearance of the image is linked to the coherence of the beam. The speckles are elongated in the q direction as the aspect ratio of the image is not preserved here.

It has been predicted and experimentally verified that the x-ray line shape of LC-aerosil samples is well fit by the sum of two terms: a Lorentzian that describes the thermal fluctuations of the LC component [26] and a squared Lorentzian that describes the static fluctuations of the quenched random disorder due to the silica network [1,27]. The squared Lorentzian is the most important contribution deep in the smectic phase, showing the importance of the disorder in reducing the smectic correlations and destroying the quasi-long-range order [28]. As pointed out in Ref. [29], the powder averaging of the squared Lorentzian reduces to a single Lorentzian if the ratio between the smectic correlation lengths in the directions parallel $\xi_\parallel$ and perpendicular $\xi_\perp$ to the nematic director is small enough and if both quantities are large enough. This is the case for our data, as expected from a comparison with previous experiments on aligned 8CB-aerosil systems [1,12] and as can be seen in Fig. 3 (sharp peak in q).

The small beam size obtained using synchrotron radiation and the high resolution of the CCD detector permitted us to achieve a much higher spatial resolution than obtained in previous studies and thus to investigate spatial heterogeneity in the smectic order. We see pronounced heterogeneities in the local LC alignment: Adjacent probed regions display rather different scattering intensities and widths. This is observable in Fig. 4, where the intensity under the peak is plotted as a function of the horizontal position on the sample. The heterogeneity is lost if the averaging is made on bigger regions,

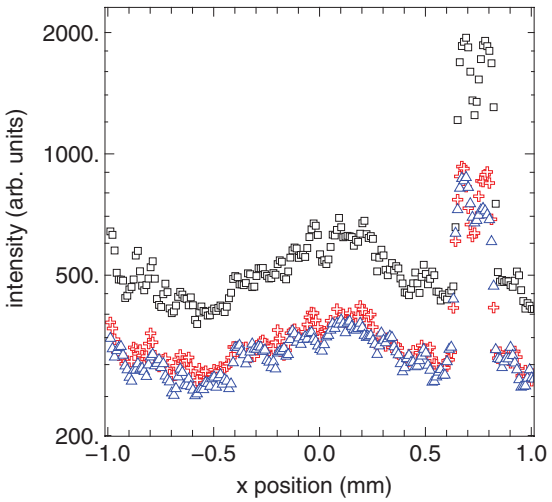

FIG. 4. (Color online) Integrated intensity in q and ϕ at 25 °C as a function of the horizontal position for 8CB with 0.059 g cm^{-3} of aerosil before the zero-field temperature cycle [(black) squares], after heating the sample to the N phase (37 °C) [(red) crosses], and after heating the sample to the isotropic phase (46 °C) [(blue) triangles].

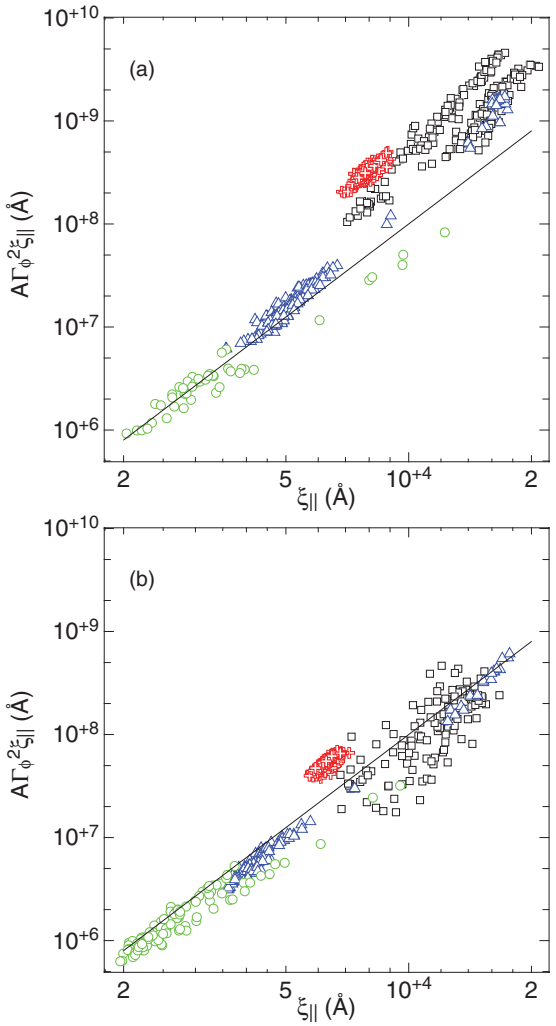

FIG. 5. (Color online) Integrated volume $A\xi_\parallel\Gamma_\phi^2$ versus $\xi_\parallel$ for the no-gel sample [(black) squares], 8CB with 0.035 g cm^{-3} of aerosil [(red) crosses], 8CB with 0.059 g cm^{-3} of aerosil [(blue) triangles], and 8CB with 0.091 g cm^{-3} of aerosil [(green) circles] at 25 °C (a) before and (b) after zero-field temperature cycles into the nematic or isotropic phase (except for the no-gel sample, which was cycled in field). Each symbol corresponds to one of the 200 (20 × 20)-μm^2 regions with the exclusion of the invalid data points. The line displays the relation $A\xi_\parallel\Gamma_\phi^2 = 1 \times 10^{-4}\ \xi_\parallel^3$.

as was the case using a (1 × 1)-mm^2 beam on aligned samples [12]. In Table I we quote the average parallel correlation length obtained from a combination of all scans. These values, which vary in the soft-gel regime from approximately 7900 Å for 8CB with 0.035 g cm^{-3} of aerosil to 3200 Å for 8CB with 0.091 g cm^{-3} of aerosil, fall closely in line with the values quoted in Ref. [12] and also with the results in Ref. [28] on unaligned gels. Thus, when viewed over a larger spatial scale, the results are consistent with earlier reports. Figures 5(a) and 5(b) present the variation of the integrated intensity A times the peak integrated volume $\xi_\parallel\Gamma_\phi^2$ as a function of the correlation length $\xi_\parallel$ for different silica concentrations obtained from a fit of the peak measured in 200 regions on the samples. They respectively correspond to the results of the fits at 25 °C before and after zero-field temperature cycles (except for the no-gel sample as described in Sec. II D). In both cases, the intensity increases with the correlation length $\xi_\parallel$, that is, as the domain size gets larger. The fact that the scattering from the different concentrations follows the same power-law variation in Fig. 5(b) seems to be consistent with the local variation in silica density, probably arising from the structure of the aerosil gels, which are known to have a broad distribution of pore sizes. The regions poorer in silica would be more likely to have larger pore size, thus permitting the LC domains to be larger. Overall, the local silica density of the samples is a varying quantity that may be different from the nominal value. A power-law variation of exponent 3 is observed and indicated by a solid line in both graphs.

The dependence of the mosaic spread defined by Γ_ϕ as a function of $\xi_\parallel$ at 25 °C before zero-field cycling is presented in Fig. 6. The power-law variation of exponent 1.5 is the sign that both characteristics are proportional: As the domains gets larger in the direction parallel to the density wave less disorder is found in the liquid direction, leading to fewer smectic layers being misoriented and scattering at other angles. This is probably related to the smectic stiffness and may be important information for the study of other smectic materials. This also implies a very interesting point. In random-field theories, the correlation length is found to be inversely proportional to the strength of the random-field disorder Δ [30]. The observed data are thus leading us to the conclusion that the ability to train the samples, as measured by the mosaic spread, goes as $\Delta^{-1.5}$.

Concerning the variation of the integrated volume with respect to $\xi_\parallel$ (Fig. 5), the exponent 3 therefore indicates that the integrated intensity varies as $\xi_\parallel^{-1}$ [31]. This power-law variation indicates that the amplitude of the static term that describes the disorder varies as $\xi_\parallel^{-1}$ and is thus inversely proportional to the disorder strength.

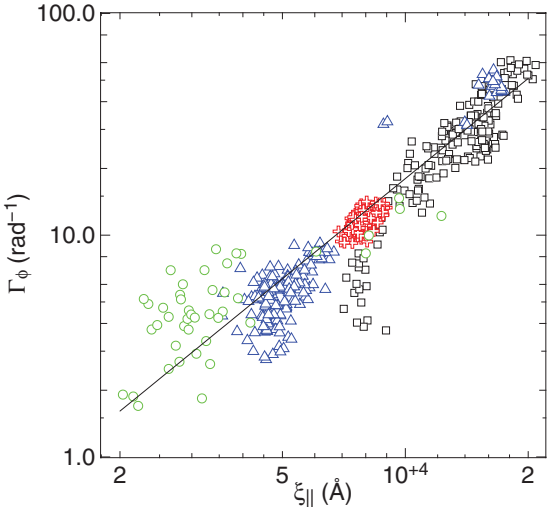

FIG. 6. (Color online) Correlation lengths Γ_ϕ versus $\xi_\parallel$ for the no-gel sample [(black) squares], 8CB with 0.035 g cm^{-3} of aerosil [(red) crosses], 8CB with 0.059 g cm^{-3} of aerosil [(blue) triangles], and 8CB with 0.091 g cm^{-3} of aerosil [(green) circles] at 25 °C before zero-field temperature cycles. Each symbol corresponds to one of the 200 (20 × 20)-μm^2 regions with the exclusion of the invalid data points. The line displays the relation $\Gamma_\phi = 1.8 \times 10^{-5}\ \xi_\parallel^{1.5}$.

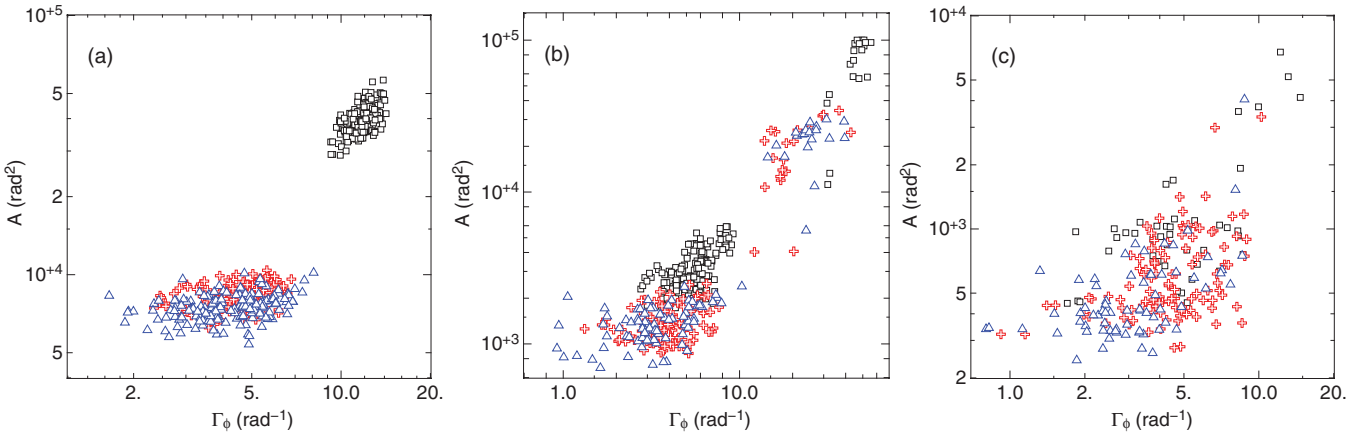

FIG. 7. (Color online) Integrated intensity versus Γ_ϕ for (a) 8CB with 0.035 g cm^{-3} of aerosil, (b) 8CB with 0.059 g cm^{-3} of aerosil, and (c) 8CB with 0.091 g cm^{-3} of aerosil at 25 °C before the first zero-field temperature cycle [(black) squares], after the first zero-field temperature cycle (up to 37 °C for 8CB with 0.035 and 8CB with 0.059 g cm^{-3} of aerosil and up to 46 °C for 8CB with 0.091 g cm^{-3} of aerosil) [(red) crosses], and after a second zero-field temperature cycle (up to 46 °C for 8CB with 0.035 and 8CB with 0.059 g cm^{-3} of aerosil and up to 80 °C for 8CB with 0.091 g cm^{-3} of aerosil) [(blue) triangles].

Interestingly, the heterogeneity at the microscopic scale was conserved after the zero-field temperature cycles, as can be seen in Figs. 5(b) and 7. Figure 5(b) shows the variation of the integrated volume after heating the samples deep into the nematic phase (37 °C) or into the isotropic phase for the no-gel sample (in the presence of the magnetic field) and the stiffest gel 8CB with 0.091 g cm^{-3} of aerosil (46 °C). The peak characteristics are similar after another run in temperature up to the isotropic phase (46 °C, or 80 °C for 8CB with 0.091 g cm^{-3} of aerosil), as can be seen in Fig. 7, where A is plotted versus Γ_ϕ before and after these two zero-field cycles. It is remarkable that the characteristics of the samples are more altered after a first run to the nematic phase than after a second run to the isotropic phase. It is also interesting to note that the loss in intensity and correlation length is more important when the gel is the softest (which nevertheless stays more aligned than the stiffer gels after temperature cycles out of the field). It thus seems that the stiffer gels are more difficult to align but are afterward more difficult to misalign. It should also be noted that the (20 × 20)-μm^2 regions that are better oriented before the temperature cycles stay better oriented after and the ones poorly oriented stay poorly oriented (cf. Fig. 4). This is another sign that the regions are defined by their local network density which does not vary from cycle to cycle.

B. Silica network structure and stability: SAXS

Small-angle x-ray scattering was also performed on 8CB-aerosil samples to see the contribution of the silica network and detect if any anisotropy in the scattering was visible. The SAXS data performed on 8CB with 0.03 and 8CB with 0.2 g cm^{-3} of aerosil after ∼10 in-field cycles in temperature show no anisotropy in the scattering for a spatial range of 123–1571 Å. The sample of 8CB with 0.059 g cm^{-3} of aerosil after 45 in-field cycles was probed at length scales between 253 and 3935 Å and did not show any anisotropy, as can be seen in Fig. 8, where the data collected for five different azimuthal directions are plotted. The small fluctuations in the intensity at low wave vectors are related to a incomplete averaging of the speckles due to the coherent beam and to different statistics close to the beam stop. The length scales probed are of relevance as they embed the mean aerosil void size for the soft-gel regime, as can be found in Table I. We also found that a fractal dimension close to 2.1 is consistent with our data [16]. The isotropy in the scattering confirms the data obtained on soft- and stiff-gel samples cycled 100 times in temperature in a 2-T field for a spatial range between 12 and 2094 Å [12].

In a similar way to what is presented in Fig. 4, the integrated intensity as a function of the vertical position of overlapping regions is presented in Fig. 9. The data shown correspond to the intensity at 25 °C after alignment and after a temperature cycle up to 46 °C. The intensity at 46 °C is also shown, where the higher overall integrated intensity reflects a thermal increase in the electron density fluctuations. The variation in intensity at 25 °C is overall similar before and after zero-field cooling, showing that the distribution of the silica network is not strongly affected by the heating to the isotropic phase of the LC. This is also confirmed by the similar signature of the network scattering at 46 °C. The restructuring of the soft-gel in the LC isotropic phase does not seem to be so important and is consistent with the results deduced from Fig. 4. It is also consistent with the findings reported in Ref. [32] that an in-field heating to the LC isotropic phase did not change the percentage of domains alignable by the field, meaning that there was no visible sign of breaking of silica strands. Finally, it supports the picture that there is a spatial variation in the silica density of the samples.

V. DISCUSSION

As can be seen in Figs. 5 and 7, two contributions to the orientational order are present in the LC-aerosil systems. One, which is more of an orientational stability than a memory effect, is lost after cycling to the N phase and is most clearly observed at low silica density. This excess orientational stability is observed as an extra scattering intensity when compared to that predicted by scaling from smaller domains,

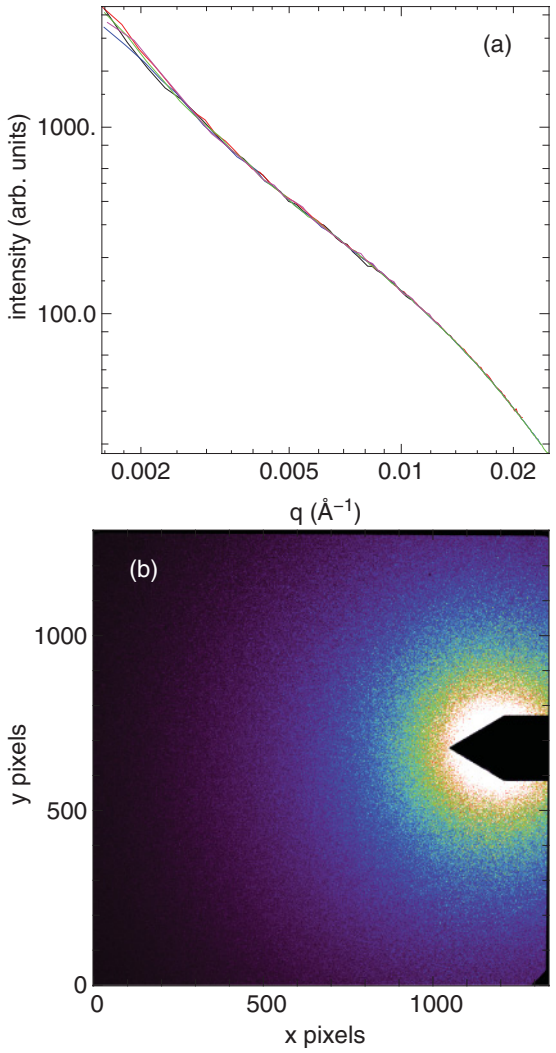

FIG. 8. (Color online) (a) Static scattering versus q for 8CB with 0.059 g cm^{-3} of aerosil at 25 °C. The five azimuthal directions analyzed here correspond to binning by 50°, from 50° to 300°, where 0° is the vertical direction and 180° is the LC alignment direction. (b) Corresponding geometry.

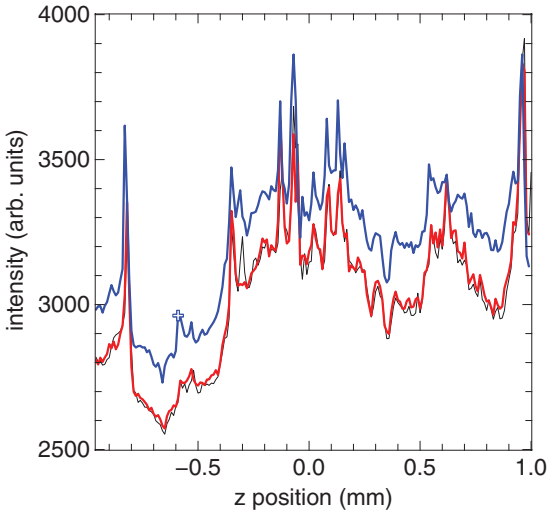

FIG. 9. (Color online) Intensity integrated over the q range 0.0016–0.025 Å^{-1} as a function of vertical position for 8CB with 0.059 g cm^{-3} of aerosil. The two lower lines correspond to the data taken at 25°C before [thin (black) line] and after [thick (red) line] the zero-field temperature cycle. The higher thick (blue) line (with a cross at $z = -0.6$) corresponds to the data taken at 46°C.

as observed in Fig. 5(a). The other, a more permanent type of memory, is preserved after a zero-field temperature cycle [cf. Figs. 5(b) and 7]. This remaining alignment seems very difficult to erase and is consistent with the locked-in structure observed by NMR for soft and stiff gels [2]. The orientational order attributed to this permanent memory depends on the local aerosil density and cannot be attributed to the pinning of line defects or to any anisotropy of the gel detectable by SAXS. This part of the memory is *trainable* by cycling in a field, which becomes less efficient with increasing gel density. To try to understand this, the description of the various steps encountered (creation, training, and erasure cycling) and their effects on the system and on the presence and distribution of defect lines are first considered followed by an estimate of two limiting lengths.

When the composite system is initially created, the evaporation of the solvent in the LC isotropic phase and the subsequent cooling down lead to an orientationally disordered nematic phase and smectic phase. Defect lines are generated in between N domains of different orientations, which are restricted from growing beyond a certain size due to the presence of the silica network. When these samples are subjected to the first in-field temperature cycle, the cooling from the isotropic phase in the presence of the magnetic field induces a preferential orientation of the director and the N domains get oriented by the alignment. Defect lines are now formed while the N arrangement favors a preferential direction. The low mobility of the defects due to the large smectic viscosity and pinning by the gel presumably causes the nematic order to retain its preferred direction even after removal of the magnetic field. When the samples are subjected to additional in-field temperature cycles, a training takes place, as evidenced by the decrease of the angular spread with the number of cycles (see Fig. 2).

The first time the trained samples are probed by microbeam XRD, before any zero-field temperature cycle, one observes an optimized orientational order attained by a compromise between the magnetic-field ordering and the disordering by the silica network. The orientational order is greatest for a small silica density where the LC domains are larger. It is also observed that the density of the aerosil network varies on a length scale of several micrometers and the orientational order follows this local variation in density. When the LC is heated to the less viscous and ordered N phase, without the presence of an aligning field, some of the orientational order is lost. There, the defects either change or relax to the local elastic minimum, which is obtained when they run along lines of largest negative Gaussian curvature [13]. This corresponds to the thermally erasable memory effect. Intuitively, it is more likely to affect samples with small silica density, as samples with higher silica density have a larger topological frustration, implying a high-energy barrier between different defect lines trajectories, that is, between different metastable states. After this first excursion into the N phase, the collapse of the data on a power-law

variation as observed in Fig. 5(b) implies that the gels of different silica density are similar systems differing only by the local amount of silica. It is worth mentioning that the loss of orientational order we observe occurs after a run to the nematic phase and not to the isotropic phase as described in Refs. [6,7], where the LC probed did not have a smectic phase. After the memory due to the pinned defect lines has been erased, the degree of the remaining LC orientational order decreases with the silica density. Note that at low enough aerosil density, the aerosil network does not percolate the system and no gel is formed.

The origin of this permanent orientational memory is considered next. In view of the trends observed for in-field cycling, a hypothesis that changes in the LC-aerosil interfacial layer are the source of the permanent alignment memory is proposed. Within a range of 100–4000 Å as probed by SAXS, no anisotropy exists in the aerosil network, but changes in the LC surface layer induced by the field must not only be remembered from cycle to cycle but improve to explain the observed training. Evidence for an oriented LC surface layer is provided by a permanent nonzero order parameter observed via a broadening of the isotropic NMR line shape in the silica dispersions [2,33], which increases linearly with the silica density, reflecting the amount of LC anchored at the surface [16].

The data presented indicate that LC surface alignment on the strands of the silica network seems to be at the origin of the observed effects. However, a *simple* surface alignment on these strands would tend to compete with the long-range orientational order and not explain the observed training effect. Indeed, the strands are isotropically oriented as found by SAXS. The lower orientational order and loss of training at high density are further strong evidence of the isotropic nature of the gel orientational effects. Thus the decrease of the angular spread with the number of cycles must be linked to another, anisotropic mechanism. We propose that intersections between gel strands are of importance in explaining the phenomenon. At intersections, the LC surface layers must comply with incompatible boundary conditions in a constrained space. As training cycles are performed, a cooperative process between the bulk LC that is easily aligned by a magnetic field and the LC surface layers at intersection points can be envisaged. A similar mechanism was proposed in [34] to account for the strong memory effects observed in LC films. Following this training process, the LC surface layers at these points of intersection would subsequently act as sites from which the LC orientational order would grow. A small anisotropy in the silica network at these points may even be imagined as their low concentration would make them difficult to observe by SAXS. Liquid crystal alignment is indeed sensitive to anisotropy in the surface morphology of a substrate down to the submicrometer length scale, aligning preferentially along the direction of lower surface roughness with an anisotropy of only 10 Å [35]. The surface memory effect has been widely observed for various LC surface combinations and may be related to the much higher transition temperature for the surface layer [36].

Naively, it can be expected that the proposed mechanism of the surface memory effect at these intersection points would lead to a stronger permanent memory at higher silica density where the number of intersections is larger. However, it seems that two limiting length scales that define the permanent memory effect can be estimated. A first limiting case occurs at high silica density and small pores sizes. It is known that finite-size effects are present below a certain domain size [37]. To estimate this limiting size, let us compare the surface energy of the system to the magnetic energy. The surface energy should go as $W_0 l_0^2$, while the magnetic energy should go as $\Delta\chi B^2 l_0^3/\mu_0$, where W_0 is the surface anchoring strength, B is the magnetic induction, and $\Delta\chi$ is the magnetic susceptibility anisotropy, which is close to 1.5×10^{-6} for 8CB. The ratio of these energies defines a length d, which could be compared with the mean void size l_0 whose values are indicated in Table I. For an expected value of W_0 around 10^{-4}–10^{-5} J m^{-2} [10,33], d should range from ~0.1 to 1 μm. At void size smaller than d, the magnetic field is not strong enough to overcome the disorder induced by the surface and the LC molecules would not tend to align with it. The director field, however, can be affected by the magnetic field in cavities larger than d. This is probably the case for the softer gels and to some extent for the stiffer end of the soft gels since the pore size distribution is broad [33] and the voids are highly interconnected. The portion of smaller domains, which are more likely to stay disordered in the presence of a field, increases with the silica density, making the higher-density dispersions more difficult to align by in-field cooling.

The other limiting case happens at low silica density and large pores sizes. For large enough pores, the number of intersections from which the alignment would grow may not be large enough to align the LC molecules in the bulk. The lower-silica-density samples would posses a higher percentage of these domains that easily lose their alignment. Soft gels such as 8CB with 0.035 g cm^{-3} of aerosil nevertheless possess a high percentage of domains with size in between these limiting lengths and present the best permanent memory. At lower silica density, but above the gelation, it can be envisaged that the number of domains with thermally erasable memory is larger than the number of domains with permanent memory and that the LC orientational order after zero-field temperature cycle would be less.

VI. CONCLUSION

The development and stability of the field memory of 8CB-aerosil dispersions to zero-field temperature cycling were studied, respectively, by NMR and microbeam XRD as a function of silica density. The permanent alignment, which increased to a steady-state value by in-field temperature cycling, is proposed to arise from training of the surface layer of the LC located at intersection points of the silica strands that make up the aerosil network. The networks are heterogeneous and composed of pores of various sizes. The LC in the larger pore sizes, which is also associated with an erasable memory, is more highly aligned due to a compromise between the number of intersection points in the network with trainable LC surface layers and the disordering effect due to a high confinement and surface energy.

For future work, a more thorough investigation of the training effect by NMR with various angles between the preferential direction and the magnetic-field direction could be envisaged, with the purpose of better understanding the training and gaining a more complete comparison with the

orientational order obtained by XRD. The training could also be made *in situ* while performing a microbeam XRD experiment to gain insight on the process of creation and distribution of aligned domains as a function of silica density. In addition, as a coherent x-ray source was used to perform the microbeam XRD experiments, information on the dynamics of the system can be extracted with the technique of x-ray photon correlation spectroscopy.

ACKNOWLEDGMENTS

We wish to thank S. Narayanan, A. Sandy, and J. Strzalka at sector 8-ID for their assistance. Use of the Advanced Photon Source was supported by the US Department of Energy, Office of Science, Office of Basic Energy Sciences, under Contract No. DE-AC02-06CH11357. Funding was also provided by the National Science Foundation (Grant No. DMR-0706021).

[1] D. Liang and R. L. Leheny, Phys. Rev. E **75**, 031705 (2007).
[2] T. Jin and D. Finotello, Phys. Rev. E **69**, 041704 (2004).
[3] R. Eidenschink and W. H. de Jeu, Electron. Lett. **27**, 1195 (1991).
[4] M. Kreuzer, T. Tschudi, W. H. de Jeu, and R. Eidenschink, Appl. Phys. Lett. **62**, 1712 (1993).
[5] A. Glushchenko, H. Kresse, V. Reshetnyak, Y. Reznikov, and O. Yaroshchuk, Liq. Cryst. **23**, 241 (1997).
[6] M. Rotunno, M. Buscaglia, C. Chiccoli, F. Mantegazza, P. Pasini, T. Bellini, and C. Zannoni, Phys. Rev. Lett. **94**, 097802 (2005).
[7] M. Buscaglia, T. Bellini, C. Chiccoli, F. Mantegazza, P. Pasini, M. Rotunno, and C. Zannoni, Phys. Rev. E **74**, 011706 (2006).
[8] R. Guo, Y. Reznikov, K. Slyusarenko, and S. Kumar, Appl. Phys. Lett. **92**, 121911 (2008).
[9] A. B. Nych, D. Y. Reznikov, O. P. Boiko, V. G. Nazarenko, V. M. Pergamenshchik, and P. Bos, Europhys. Lett. **81**, 16001 (2008).
[10] A. Jákli, L. Almásy, S. Borbély, and L. Rosta, Eur. Phys. J. B **10**, 509 (1999).
[11] P. G. de Gennes and J. Prost, *The Physics of Liquid Crystals*, 2nd ed. (Oxford University Press, New York, 1995).
[12] D. Liang, M. A. Borthwick, and R. L. Leheny, J. Phys. Condens. Matter **16**, S1989 (2004).
[13] T. Araki, M. Buscaglia, T. Bellini, and H. Tanaka, Nature Mater. **10**, 303 (2011).
[14] D. Sharma, J. C. MacDonald, and G. S. Iannacchione, J. Phys. Chem. B **110**, 16679 (2006).
[15] S. Frunza, L. Frunza, H. Goering, H. Sturm, and A. Schönhals, Europhys. Lett. **56**, 801 (2001).
[16] G. S. Iannacchione, C. W. Garland, J. T. Mang, and T. P. Rieker, Phys. Rev. E **58**, 5966 (1998).
[17] J. Als-Nielsen, J. D. Litster, R. J. Birgeneau, M. Kaplan, C. R. Safinya, A. Lindegaard-Andersen, and S. Mathiesen, Phys. Rev. B **22**, 312 (1980).
[18] J. Seelig, Q. Rev. Biophys. **10**, 353 (1977).
[19] In cases where there is a rotational symmetry about zero, the director orientation should also include a volume element $\sin\theta$ leading to a singular point at $\theta = 0^\circ$. However, including $\sin\theta$ does not lead to the sharp features observed at $\theta = 0^\circ$. We found that a simple Gaussian probability distribution gave better fits to our data [23].
[20] A. Arcioni, C. Bacchiocchi, L. Grossi, A. Nicolini, and C. Zannoni, J. Phys. Chem. **106**, 9245 (2002).
[21] S. A. Brooks, G. R. Luckhurst, and G. F. Pedulli, Chem. Phys. Lett. **11**, 159 (1971).
[22] S. Kumar, *Liquid Crystals: Experimental Study of Physical Properties and Phase Transitions*, Chap. 3 (Cambridge University Press, Cambridge, 2001).
[23] R. Stannarius, G. P. Crawford, L. C. Chien, and J. W. Doane, J. Appl. Phys. **70**, 135 (1991).
[24] Γ_ϕ is squared as the two liquid directions are equivalent and should have the same broadening.
[25] B. M. Ocko, R. J. Birgeneau, and J. D. Litster, Z. Phys. B **62**, 487 (1986).
[26] J. Als-Nielsen, R. J. Birgeneau, M. Kaplan, J. D. Litster, and C. R. Safinya, Phys. Rev. Lett. **39**, 352 (1977).
[27] S. Park, R. L. Leheny, R. J. Birgeneau, J.-L. Gallani, C. W. Garland, and G. S. Iannacchione, Phys. Rev. E **65**, 050703 (2002).
[28] R. L. Leheny, S. Park, R. J. Birgeneau, J.-L. Gallani, C. W. Garland, and G. S. Iannacchione, Phys. Rev. E **67**, 011708 (2003).
[29] T. Bellini, L. Radzihovsky, J. Toner, and N. A. Clark, Science **294**, 1074 (2001).
[30] L. Radzihovsky and J. Toner, Phys. Rev. B **60**, 206 (1999).
[31] The data provide clearer evidence this way rather than by directly plotting A versus $\xi_\parallel^{-1}$, probably due to a reduction in the noise.
[32] C. T. Yim, Phys. Rev. E **80**, 031704 (2009).
[33] S. Kralj, G. Lahajnar, A. Zidanšek, N. Vrbančič-Kopač, M. Vilfan, R. Blinc, and M. Kosec, Phys. Rev. E **48**, 340 (1993).
[34] D. M. Scott, N. A. Smith, J. J. Valente, R. Adams, K. Bufkin, and D. L. Patrick, J. Phys. Chem. **114**, 1810 (2010).
[35] S. Kumar, J.-H. Kim, and Y. Shi, Phys. Rev. Lett. **94**, 077803 (2005).
[36] Y. Shi, B. Cull, and S. Kumar, Phys. Rev. Lett. **71**, 2773 (1993).
[37] S. Kralj, A. Zidanšek, G. Lahajnar, I. Muševič, S. Žumer, R. Blinc, and M. M. Pintar, Phys. Rev. E **53**, 3629 (1996).